Morphology and Volatility of Particulate Matter Emitted from a Gasoline Direct Injection Engine Fuelled on Gasoline and Ethanol Blends

Brian Mackenzie Graves, Charles Robert Koch, Jason Scott Olfert[a]

Department of Mechanical Engineering, University of Alberta
Mechanical Engineering Building, University of Alberta, Edmonton, AB, T6G 2G8, Canada

[a]Corresponding author, jolfert@ualberta.ca

Abstract

The particulate matter emitted from a turbocharged, four cylinder, wall-guided, gasoline direct injection (GDI) engine fuelled with gasoline and ethanol blends was investigated, and characterized by size distribution, mass-mobility exponent, effective density, and volatility using tandem measurements from differential mobility analysers (DMA) and a centrifugal particle mass analyser (CPMA). Three engine loads were tested at 2250 RPM (4%, 13%, and 26% of maximum load) in addition to an idle condition while the engine was fuelled using gasoline mixed with ethanol fractions of 0% (E0), 10% (E10), and 50% (E50) by volume. An increase in engine load increased particle number concentration, although idle produced approximately as many particles as at 13% load. In the majority of cases, an increase in ethanol fraction decreased number concentration. The fraction of the number of particles comprised of only volatile material to total number of particles (number volatile fraction) both overall and as a function of particle mobility-equivalent diameter was under 10 percent at all engine conditions and fuels (measured after a three-way catalytic converter). The size-segregated ratio of the mass of internally mixed volatile material to total particle mass was similarly low. Volatility measurements were conducted using a thermodenuder set to 300°C. Mass-mobility exponent was seen to range between 2.28 and 2.60. Effective density increased with load, and in general mass-mobility exponent increased as well. Effective density decreased with an increase in ethanol fraction and a slight decrease in mass-mobility exponent was also observed for all conditions except idle. No significant changes in effective density, particle size, or number concentration were observed in GDI soot after denuding particle samples.

1. Introduction

The introduction of direct fuel injection to gasoline engines has led to an increase in fuel efficiency and engine performance in relation to traditional port injection. This is because direct injection allows for control of fuel injection timing, and because the liquid droplets sprayed into the cylinder cool the surrounding air as they evaporate, which then allows more air into the cylinder. Unfortunately, these liquid fuel droplets also have less time to evaporate and mix with the incoming air, so particulate emissions of direct injection engines tend to be higher than those from port injection engines (Su et al., 2013; Liang et al., 2013; Karavalakis et al., 2014; Bielaczyc et al., 2014, Short et al., 2015).

The addition of ethanol to gasoline has advantages which include increased knock resistance and potential greenhouse gas benefits because ethanol is typically produced from renewable sources (U.S. Department of Energy, 2015). Moreover, there is evidence that ethanol reduces PM emissions (Fatouraie et al., 2013; Storey et al., 2014; and Zhang et al., 2014). A maximum fraction of 10% ethanol is allowed by the EPA to be blended with gasoline for use in all cars and light trucks, although the EPA has approved the use of 15% ethanol in vehicles of model year 2001 and newer (EIA, 2012). Ethanol consumption in the US is proposed to be 13.71 billion gallons in 2015 and 13.83 billion gallons in 2016 (up from 13.47 billion gallons in 2014 and 12.86 billion gallons in 2010) (EIA, 2015a; EIA, 2015b). One challenge facing the introduction of higher-percentage ethanol mixtures is its compatibility with materials used within engines. Vehicles compatible with ethanol will need to be commonplace if its content in gasoline is to increase significantly (EIA, 2012).

Blending ethanol into gasoline has been shown to either increase or decrease PM emissions for GDI engines. The oxygen contained in ethanol is thought to help oxidize particles and ultimately reduce PM emissions (Chen et al., 2012). Moreover, aromatic molecules have been linked to PM production (Vuk and Vander Griend, 2013; Chen et al., 2015) and the addition of ethanol leads to a fuel mixture with a smaller aromatic fraction than pure gasoline. Ethanol has been found to decrease particulate number and mass concentrations by Storey et al. (2010), Storey et al. (2012), Catapano et al. (2013), Vuk and Vander Griend (2013), Fatouraie et al., (2013), Storey et al. (2014), and Zhang et al. (2014). Despite this, there is also conflicting evidence that ethanol can increase particulate production in some instances (Chen et al., 2010; Chen et al., 2012; Catapano et al., 2013). This is suspected to be due to the higher heat of vaporization of ethanol in relation to gasoline, meaning that fuel droplets take longer to evaporate and the air-fuel mixture becomes less well mixed, leading to zones of fuel-rich combustion (Chen et al., 2012). Similar effects from the aromatic content and volatility of the gasoline itself have been observed by Khalek et al., (2010), Kim et al. (2013), and Storey et al. (2014). Other alcohols have also been

investigated such as butanol, which decreased PM when mixed with gasoline (Gu et al., 2012; Zhang et al., 2014; Karavalakis et al., 2014); although it also decreases the fuel's knock resistance. Liang et al. (2013) investigated blends of gasoline mixed with methanol and found that methanol also helps reduce PM emissions. The varying results from these studies regarding the increase or decrease of PM production could also be attributed variations in other parameters such as gasoline composition, engine operating conditions (i.e. load and speed) or injection strategy (i.e. wall-guided or spray-guided fuel injection).

The solid portion of particulate matter (PM) generated by gasoline direct injection (GDI) engines is largely comprised of elemental carbon formed into small primary particles which agglomerate to form fractal-like aggregates. Primary particle size has been shown to increase with aggregate size (Lee et al., 2013; Dastanpour and Rogak, 2014; Seong et al., 2014), and ranges from < 5 nm (Sgro et al., 2012) to 55 nm (Kameya and Lee, 2013). The shape of an aggregate particle can be quantified using the mass-mobility exponent, which describes the scaling of particle mass (m) with mobility-equivalent diameter (d_{m}),

$$m = C{d_{\mathrm{m}}}^{D_{\mathrm{m}}}, \quad (1)$$

where C is a prefactor, and D_{m} is the mass-mobility exponent. The mass-mobility exponent can be used to estimate primary particle size with aggregates (Dastanpour et al., 2015). In the case of GDI soot, Symonds et al. (2008) determined the mass-mobility exponent to be 2.65 and Momenimovahed and Olfert (2015) calculated exponents between 2.5 and 2.7 for non-volatile particles. These exponents are higher than those for typical diesel soot (2.33 - 2.41 for Park et al. (2003), 2.3 ± 0.1 for Maricq et al. (2004), and 2.22 - 2.48 for Olfert et al. (2007) when the particle volatility was low). Barone et al. (2012), Lee et al. (2013), and Kameya and Lee (2013) have noted similarities of GDI particulate to diesel particulate regarding particle shape and internal structure. The mass-mobility exponents from port fuel injection (PFI) engines have also been characterized by Quiros et al. (2015), who found values ranging from 2.45 to 2.68 for gasoline and 2.39 to 2.52 for E85. To date, a study has not been conducted on the effects of ethanol on mass-mobility exponent for GDI engines.

In addition to solid carbon, particulate may also exist in the liquid phase. Droplets can be formed from impinged fuel or oil on a surface within the cylinder (Barone et al., 2012) or from condensed hydrocarbons in the exhaust (Sgro et al., 2012; Lee et al., 2013). Liquids can form separate droplets or they can condense on the solid soot aggregates. In the latter case, the proportion of volatile material to solid carbon within a given particle is dependent on particle size. Sakurai et al. (2003) and Ristimäki et al. (2007) found that the relative amount of volatile material on a particle decreases with an increase in particle size on a volume basis and a mass basis for diesel engines. Ghazi et al. (2013) observed the same trend for particulate generated from McKenna and inverted burners, as did Graves et al. (2015) for a direct-injected natural gas compression ignition engine while at low loads. Momenimovahed and Olfert (2015) also noticed this effect on GDI engines at conditions where volatility was substantial (above approximately 20%). Depending on engine power, they observed mass-based volatility between 10% and 30%. Research has not yet been done to investigate the effects of ethanol in GDI engines on particle volatility.

In this study, tandem differential mobility analyzers (DMA) were used in conjunction with a centrifugal particle mass analyzer (CPMA) to determine the effect of ethanol on GDI particulate emissions in terms of their particle structure (size, mass-mobility exponent, and effective density) and volatility (or mixing state). Knowledge of PM structure and volatility will allow recommendations to be made regarding aftertreatment strategies (e.g. gasoline particulate filter (GPF), catalytic converter). For example, highly volatile PM emissions will necessitate catalytic treatment, whereas predominantly non-volatile PM emissions would need to be removed using filtration. Furthermore, the effective density allows the PM mass concentration to be determined using size distributions instead of time consuming filter methods which are susceptible to measurement artifacts (CARB, 2015).

2. Experimental Setup

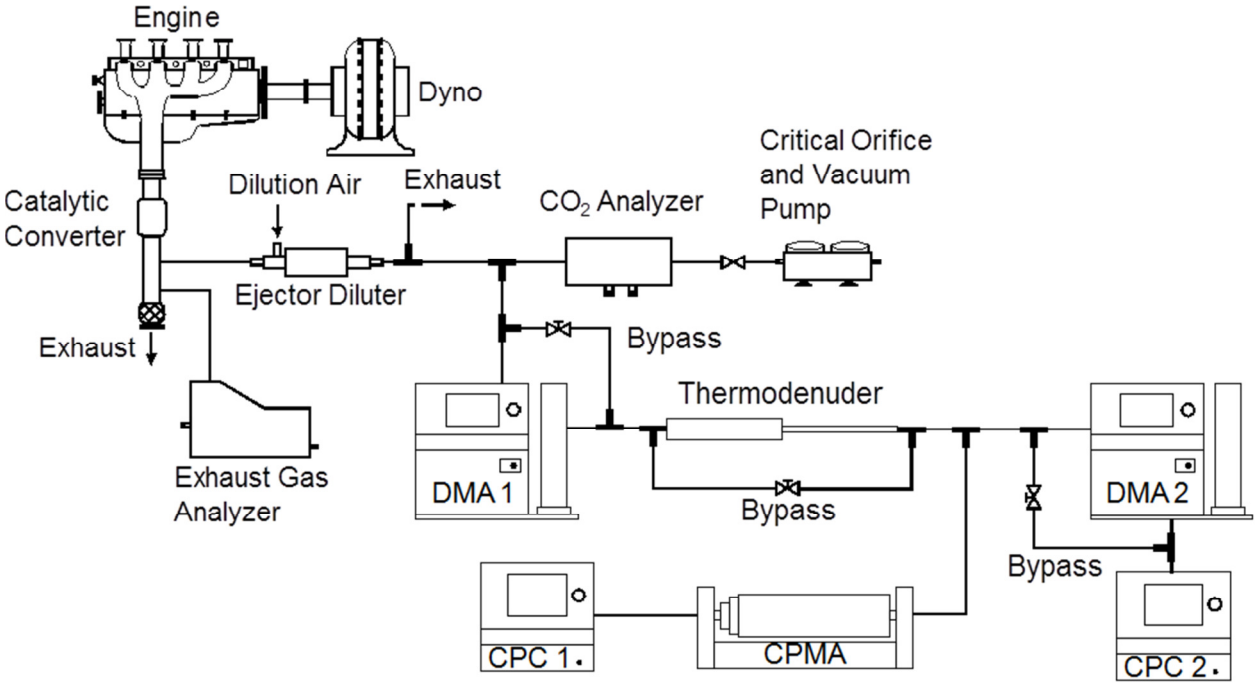

Figure 1: Experimental Setup

The experimental setup is pictured in Figure 1. Measurements were taken from the exhaust of a General Motors 2.0 litre, 4-cylinder, turbocharged, wall-guided GDI engine fitted with the production three-way catalytic converter and fuelled with gasoline mixed with 0% (E0), 10% (E10), and 50% (E50) ethanol by volume. Commercially available, ethanol-free, gasoline was used as the base fuel. The gasoline was analyzed and the results of the analysis are shown in Table 1. As expected the gasoline did not contain any oxygenates (i.e. ethanol). The most prominent constituents within the gasoline are aromatics and isoparaffins, the former is often associated with PM production. Also notable are the boiling points: the gasoline contains components which boil at both higher and lower temperatures than that of the ethanol. Ethanol does have a higher heat of vaporization however; so its charge cooling effect will be greater, and this may subsequently affect the fuel's ability to evaporate.

Table 1: Properties of gasoline and ethanol

Property	**Gasoline (Shell 91 Octane)**	**Ethanol**
Formula	C3 – C12	C_2H_5OH
Density (kg/m^3)	785	790*
Boiling Point, 10% (°C)	38.1	
Boiling Point, 50% (°C)	102.2	78*
Boiling Point, 90% (°C)	159.2	
Anti-knock index **	91	100*
Aromatic Content (Volume %)	44.3	0.0
Isoparaffin Content (Volume %)	34.6	0.0
Napthene Content (Volume %)	4.8	0.0
Olefin Content (Volume %)	0.7	0.0
Paraffin Content (Volume %)	15.1	0.0
Oxygenate Content (Volume %)	0.0	100.0

Unidentified (Volume %)	0.4	0.0

*Catapano et al., 2013

**Anti-knock index (AKI) is equal to the mean of the research octane number (RON) and motor octane number (MON)

The engine was fitted to a 250 horsepower eddy current dynamometer (Dyne Systems Inc., Model MW1014W) and operated at four steady-state loads. The engine loads tested were chosen to match engine loads that are frequently encountered during the New European Driving Cycle (NEDC) (UNECE, 2013). The most common loads were approximately 15 N m and 45 N m and were chosen as test points alongside the idle condition (800 RPM). Another load of 90 N m was chosen since it is approximately the load encountered during acceleration in the NEDC. All three loads were operated at a speed of 2250 RPM. In relation to the engine's maximum torque output at 2250 RPM of 350 N m, these loads represent 4%, 13%, and 26% of the maximum achievable load. Fuel injection during idle was at the beginning of the intake stroke (350° before top dead centre), and approximately the middle of the intake stroke while at 2250 RPM (280° before top dead centre).

Before taking measurements on a given day, the engine ran for approximately half an hour until parameters such as oil and catalyst temperatures became steady. In cases when multiple engine loads were tested without shutting the engine off, the engine was allowed to run for approximately fifteen minutes so the emissions could stabilize once again. After changing fuels, the engine was operated for at least an hour before any data was collected. Three replicate measurements were taken for each load and fuel, with the exception of size-segregated number concentrations, which were measured on one occasion but with five or six repeat measurements per size.

PM sampling was done by first passing the exhaust sample through a Dekati DI-1000 ejector diluter. A sensitivity study was conducted on the effects of heated dilution using a scanning mobility particle spectrometer (SMPS) and thermodenuder. No observable difference in the size distributions or the amount of volatile material was found for all four engine conditions. Unheated dilution was used subsequently. The dilution ratio (β) was calculated using measurements of upstream and downstream CO_2 concentration (measured by a Vetronix PXA-1100 exhaust gas analyzer and LI COR LI-840A CO_2 analyzer, respectively) and is

$$\beta = \frac{\varphi_1 - \varphi_{\mathrm{da}}}{\varphi_2 - \varphi_{\mathrm{da}}}. \quad (2)$$

φ_1 is the upstream concentration of CO_2, φ_2 is the downstream CO_2 concentration, and φ_{da} is the CO_2 concentration in the dilution air (Giechaskiel et al. 2009). The dilution ratio, which was calculated specifically for each PM measurement, was roughly 13:1.

After dilution, the flow passed into DMA1 (TSI Inc., Model 3081, Kr-85 neutralizer six years old at time of data collection) which was maintained at a constant voltage to classify particles with a narrow range of electrical mobility. The sheath flow and aerosol flow rates of DMA1 were 18 L/min and 1.8 L/min, respectively. The aerosol sample was then sent to a thermodenuder (heated to 300℃, heating section 0.665 m long, 9.50 mm inner diameter; cooling section 1.435 m long, 2.75 mm inner diameter; 0.8 second residence time in heating section for 1.8 L/min aerosol flow rate) or its bypass, at which point the flow was split. 1.5 L/min of the flow was sent to a CPMA, which classifies an aerosol based on its mass to charge ratio (Olfert and Collings, 2005). The CPMA was stepped through various particle mass settings, by changing voltage and rotation speed. This results in a resolution which does not vary with particle mass. The CPMA resolution is defined as the inverse of the normalized full-width half-maximum of the transfer function, and was approximately 10 (i.e. the resolution was approximately a tenth of the CPMA set point) where possible, but at particle sizes of 30 nm and 45 nm it was set to 5 because the rotational speed would have otherwise exceeded the classifier's limitations. Note that a mass-based resolution results in a narrower transfer function than a size-based resolution of the same value, due to the exponential scaling of mass with diameter. Particle counts were measured using a condensation particle counter (CPC; TSI Inc. Model 3776). The mass distribution function is approximately lognormal and its peak corresponds to the average classified particle mass assuming multiply charged particles are not present. A log-normal distribution, as seen in Tajima et al. (2011), was fit to the mass distribution to determine the average

particle mass at each set point. The fraction of multiply charged particles in the experiments is calculated in the supplemental information and is found to be no greater than 10%. As particle mass is determined from the peak of the CPMA scan, the presence of a small number of multiply-charged particles at a larger mass introduces little error in the peak mass determined by a fit of the mass distribution.

The remaining 0.3 L/min exiting the thermodenuder was sent to DMA2 (sheath flow 3 L/min) and CPC2, identical to the instruments mentioned above. The charge neutralizer of DMA2 was bypassed because the particles had already been charged while passing through DMA1. DMA2 was stepped through various particle sizes as CPC2 recorded the corresponding number concentration. An inversion code was applied to the data to determine the mobility-equivalent diameter of the particles (Stolzenburg and McMurry, 2008). The total particle size distribution data was also collected by conducting SMPS scans while bypassing DMA1. Number concentrations for denuded scans were corrected for diffusional and thermophoretic losses using an experimentally-determined relationship specific to the thermodenuder.

3. Experimental Results

3.1 Size Distributions

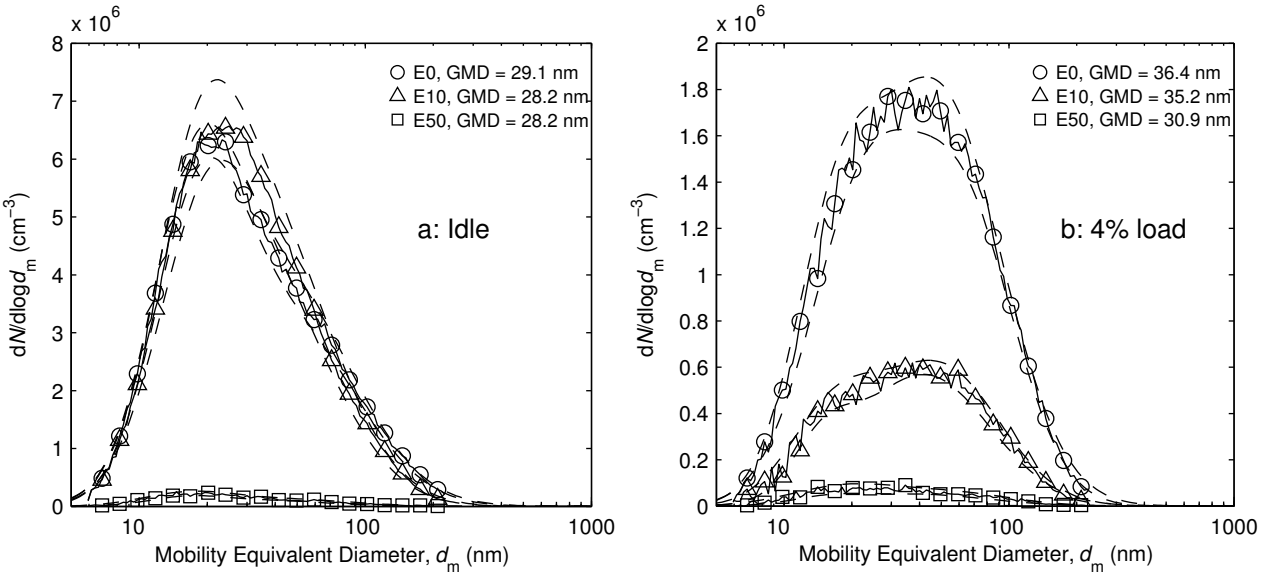

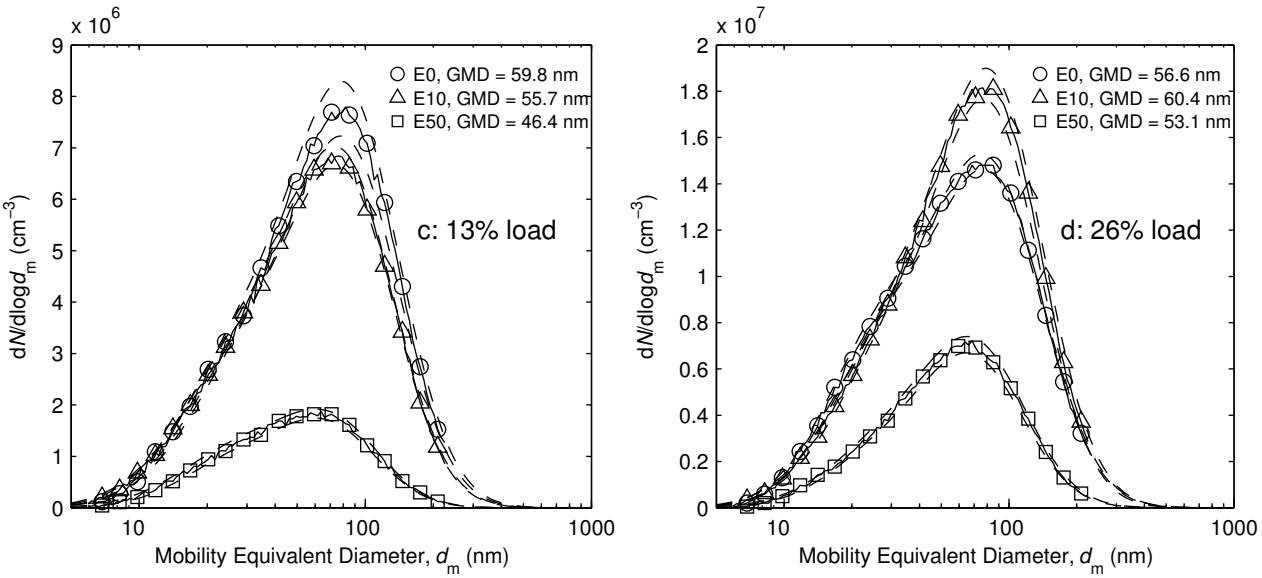

Figure 2: Undenuded particle size distributions for idle (a), 4% load (b), 13% load (c), and 26% load (d). Three replicate measurements were taken for each point except for E10 at idle, where seven measurements were taken. Dashed lines represent one standard deviation.

The undenuded size distributions for all fuels and loads are plotted in Figure 2. In relation to engine conditions, the geometric mean diameter (GMD) was lowest at idle and increased with load (GMDs at 13% load and 26% load were similar). A small decrease in GMD was observed as ethanol fraction was increased. Likewise, Zhang et al. (2014) saw a decrease in GMD as ethanol fraction increased, although Storey et al. (2010) did not see a significant change in GMD with ethanol fraction.

It is apparent from Figure 2 that the size distributions are not log-normal, but appear to be skewed. It may be possible that these distributions appear skewed because the aerosol is comprised of two log-normal distributions: a nucleation mode (with GMD of ~20 nm) and an accumulation mode (with GMD of ~80 nm). However, this terminology may not be appropriate. The terms imply that two species of PM, formed by two different mechanisms, are present within the particle size distribution. In diesel exhaust, for example, typically volatile liquids grow through nucleation into particles at small diameters (nucleation mode), while aggregates of solid particles accumulate at larger diameters (accumulation mode). As is evident in the next section, very little volatile material is present in the GDI aerosol and there is no distinction between particle morphology across the size range. The mechanism responsible for PM formation may simply result in size distributions which are not log-normal. The non-log-normal distribution shape measured here has been seen in particulate measurements from other GDI engines (Gu et al., 2012; Zhang et al., 2014; Momenimovahed and Olfert 2015).

3.2 Volatility and mixing state

The number of volatile particles removed after passing through the thermodenuder divided by the total number concentration of the sample (N_{undenude}) is known as the number volatile fraction (f_{N}). This can also be expressed using the number of non-volatile particles measured after denuding (N_{denude}):

$$f_{\text{N}} = 1 - \frac{N_{\text{denude}}}{N_{\text{undenude}}}. \quad (3)$$

This value gives a measurement of externally mixed volatility. It represents the fraction of particles which are purely volatile and contain no non-volatile material (no solid carbon cores). More accurately, the amount of non-volatile material remaining after thermodenuding results in a particle smaller than the lower detection limit of the CPC which is approximately 2.5 nm. N_{denude} and N_{undenude} are obtained by selecting a mobility-equivalent diameter using DMA1 in Figure 1 then measuring the number concentration through the heated and bypass lines of the denuder with CPC2 (while bypassing DMA2). f_{N} as a function

of mobility equivalent diameter for E0 is displayed in Figure 3 (Size-segregated f_N plots for other fuels are displayed in the online supplemental information). f_N is relatively low throughout the size range, at approximately five percent, and there is no observable trend with particle size.

Similarly, the mass volatile fraction (f_m) can be determined using separate mass measurements of denuded (m_{denude}) and undenuded particles ($m_{undenude}$) by dividing the mass of volatile material on a single particle by the total mass of that particle.

$$f_m = 1 - \frac{m_{denude}}{m_{undenude}}. \quad (4)$$

This gives a measurement of internally mixed volatility, or a comparison of volatile material to total mass of a given particle. For a given mobility-equivalent diameter selected with the first DMA, m_{denude} and $m_{undenude}$ are the average particle masses measured with the CPMA and CPC1 (Figure 1) for particles passing through the heated and bypass lines of the thermodenuder, respectively. f_m as a function of mobility equivalent diameter for E0 is shown in Figure 4 (plots for other fuels are shown in the online supplemental information). f_m trends are similar to f_N and remain under 10 percent for all loads and fuels. These results are lower than those from Momenimovahed and Olfert (2015), who determined f_m values in the range of 10% to 30%, and as the volatile fraction increased with power, a decrease with increasing particle size was observed. This negative correlation with size has also been observed in diesel engines (Sakurai et al. 2003; Ristimaki et al. 2007), inverted and McKenna burners (Ghazi et al., 2013), as well as a compression-ignition natural-gas engine (Graves et al., 2015).

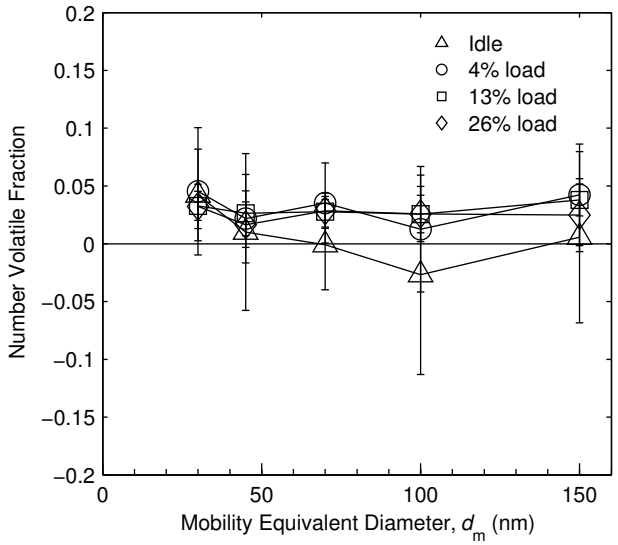

Figure 3: f_N as a function of mobility equivalent diameter for E0. Error bars represent one standard deviation.

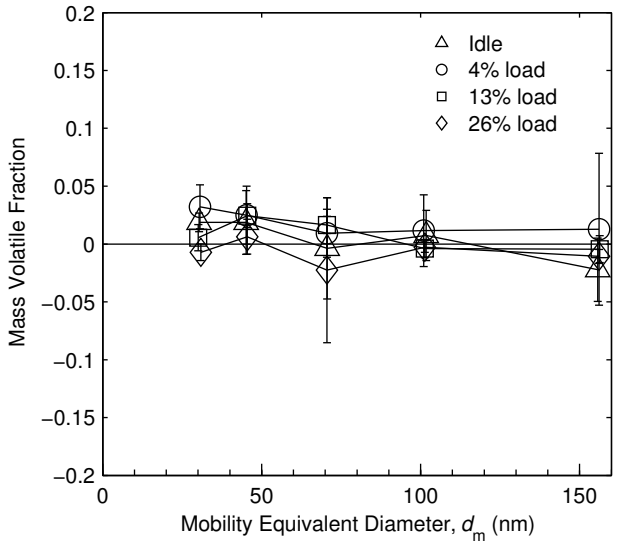

Figure 4: f_m as a function of mobility equivalent diameter for E0. Error bars represent one standard deviation.

Because the size-segregated values are relatively constant, it is sufficient to use the average values for subsequent calculations. The average f_N and f_m for each fuel and load are shown in Figure 5 and Figure 6 respectively. All fractions are seen to be under 5 percent, and the negative measurements are due primarily to variability in the engine-out particle concentration. E50 at 4% load and idle have particularly high uncertainty because their number concentrations were extremely low.

Figure 5 and Figure 6 show that there is a relatively small amount of volatile particulate emitted from the GDI engine post-catalyst. The PM emitted by the engine may already contain little volatility, but even if that is not the case, the catalyst likely oxidizes most volatile material before it is sampled. Samuel et al. (2010) found that during a cold engine start, particle count was reduced by three orders of magnitude after the catalyst, and that during a low speed, low load condition the catalyst reduced PM number by 98 percent. They also note that it is unclear whether the catalyst removes the particles directly or removes their precursors; preventing them from forming or growing. Whelan et al. (2013) also found a sharp decrease in PM number using a catalyst (65 percent reduction overall with up to 95 percent of particles smaller than 23 nm removed). They determined an effective lightoff temperature where the post-catalyst exhaust temperature is around 80 – 100°C at which point the downstream particle concentration becomes mostly steady. They note that this is significantly lower than the lightoff temperatures for carbon monoxide or hydrocarbons.

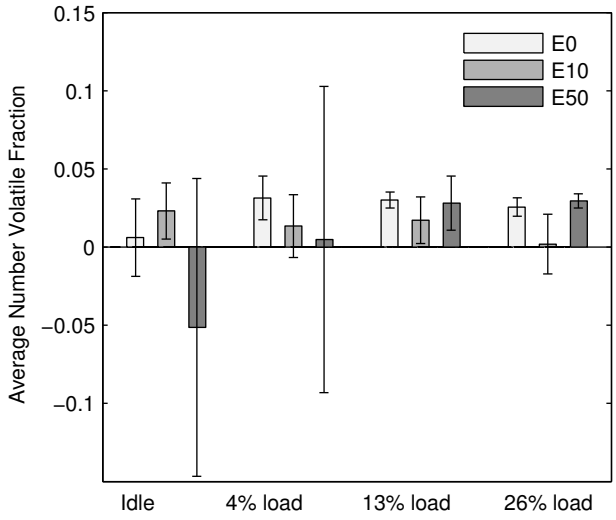

Figure 5: Average f_N for all loads and fuels. Error bars represent the standard deviation of data points of all sizes at that fuel and load.

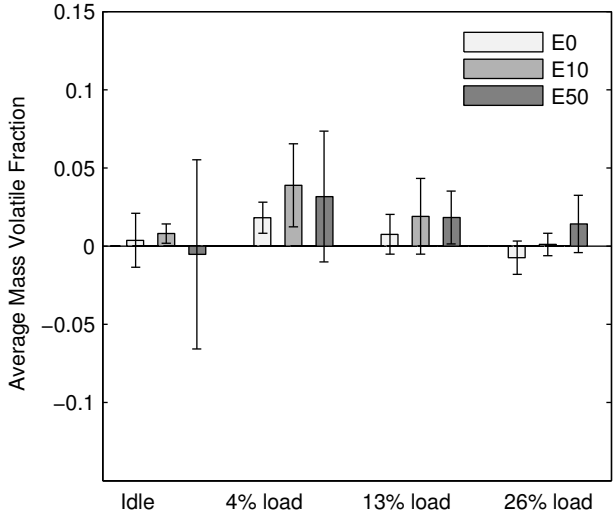

Figure 6: Average f_m for all loads and fuels. Error bars represent the standard deviation of data points of all sizes at that fuel and load.

Total number concentrations determined from integrating undenuded SMPS size distributions can be multiplied by their respective average f_N values to show the number concentrations of purely volatile particles and particles containing non-volatile solid material ($N_{volatile}$ and $N_{non\text{-}volatile}$). These parameters can be determined as

$$N_{\mathrm{volatile}} = \sum \left(\frac{\mathrm{d}N}{\mathrm{dlog}d_{\mathrm{m}}}\right)(\mathrm{dlog}d_{\mathrm{m}})f_{\mathrm{N}}\,, \tag{5}$$

and

$$N_{\mathrm{non-volatile}} = \sum \left(\frac{\mathrm{d}N}{\mathrm{dlog}d_{\mathrm{m}}}\right)(\mathrm{dlog}d_{\mathrm{m}})(1-f_{\mathrm{N}})\,, \tag{6}$$

respectively, where $\frac{\mathrm{d}N}{\mathrm{dlog}d_{\mathrm{m}}}$ is the number concentration of a given particle size bin, normalized by bin width. As shown in Figure 7, number concentration is seen to scale with load although idle produced roughly as many particles as at 13% load. Increases in PM with engine load have commonly been seen in

the literature (Maricq et al., 1999; Farron et al., 2011; Su et al., 2013; Bonatesta et al., 2014), and this is believed to be due in part to the larger quantity of fuel itself, and also due to the greater cooling effect observed from the fuel evaporation. Fuel evaporation rate may also be reduced at higher loads due to lower amounts of exhaust residuals (i.e. lower initial air/residual temperature) (Stone, 2012). Number concentrations also decreased with an increase in ethanol fraction, with the exceptions of E10 at 26% load and idle where the concentrations are equal to or slightly higher than the concentration from E0. Maricq et al. (2012) have observed similar trends, where relatively low fractions of ethanol (under 20%) showed a marginal decrease in PM production, while higher fractions (above 30%) reduced PM between 30% and 45%. Moreover, Storey et al. (2010), Storey et al. (2012), Vuk and Vander Griend (2013), and Zhang et al. (2014) also observed decreases in number concentration with the addition of ethanol. Externally mixed volatile particles (shown as the black regions at the tops of the bars) contribute little to the overall concentrations, and little trend is seen in relation to engine condition or fuel type.

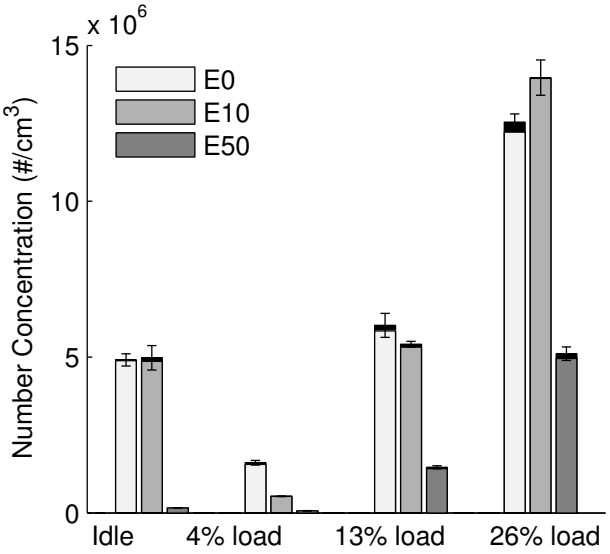

Figure 7: Total particle number concentrations. Error bars represent one standard deviation of the total number concentration. Black regions depict purely volatile particles and other shades show particles containing solid particulate.

3.3 Effective Density and Mass-Mobility Exponent

The relation between mass and mobility-equivalent diameter (Eq. 1) can be rearranged to determine particle effective density

$$\rho_{\mathrm{eff,D}} = \frac{m_D}{\frac{\pi}{6} d_{\mathrm{m,D}}{}^3} = \frac{6}{\pi} C d_{\mathrm{m,D}}{}^{D_{\mathrm{m,D}}-3} = k d_{\mathrm{m,D}}{}^{D_{\mathrm{m,D}}-3}. \quad (7)$$

The branching pattern of the aggregate particles incorporates more open space as the particle increases in size, and thus the effective density decreases accordingly. A power-law fit using masses at various mobility-equivalent diameters allows the prefactor k and exponent D_{m} to be calculated. Here the denuded mass (m_{D}) and denuded mobility diameter ($d_{\mathrm{m,D}}$) are used to explore the morphology of the soot aggregate alone (i.e. not the morphology of particles comprised of a non-volatile soot aggregate and any volatile material that may be present on the aggregate).

Denuded effective density measurements for all loads and fuels can be seen in Figure 8. Corresponding mass-mobility exponents and prefactors are listed in the legends. A two-way analysis of covariance (ANCOVA) confirmed that both engine condition and ethanol fraction indeed have small but highly statistically significant effects on effective density, with p-values << 0.001. The standard deviation of mass-mobility exponents is 0.10 and 95% of effective density data points are within 21% of a trend line fit to all data (seen in the supplemental information). As can be seen from Figure 8, these differences in effective density due to ethanol content and engine condition are very small. Mass-mobility exponent was

typically lowest at idle (2.29 – 2.43) and increased with load, although 13% load had exponents which fit inside the range of exponents observed at 26% load (2.49 to 2.60). An increase in ethanol fraction decreased effective density as well as mass-mobility exponent, except at idle. Effective densities observed here are similar to GDI engines tested by Quiros et al. (2015) and Momenimovahed and Olfert (2015), and mass-mobility exponents were also similar (2.29 to 2.52, and 2.61, respectively). The comparison with these other studies is examined in further detail in the supplemental information.

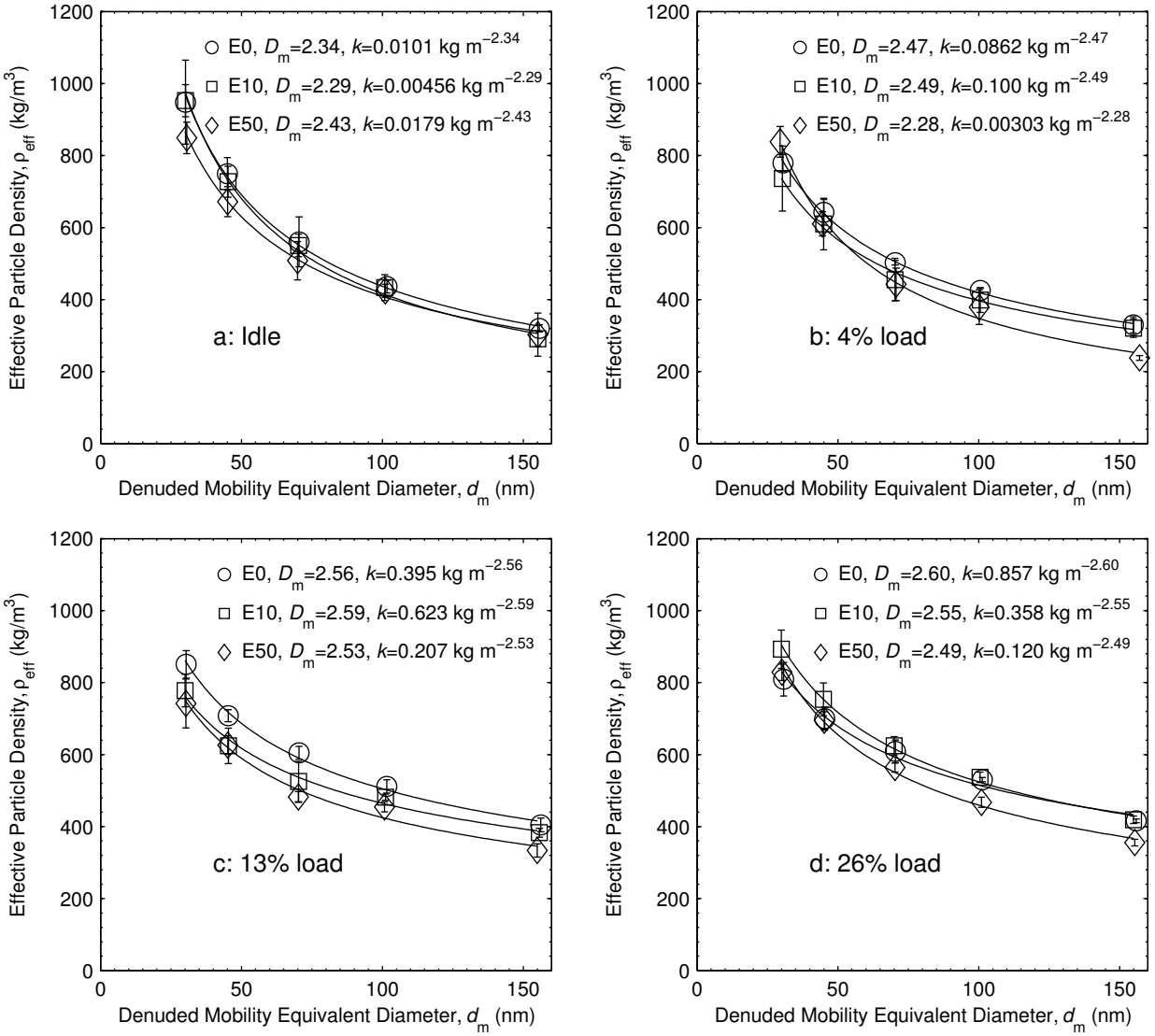

Figure 8: Denuded effective density as a function of particle mobility-equivalent diameter for idle (a), 4% load (b), 13% load (c), and 26% load (d). Three replicate measurements were taken for each point. Error bars represent one standard deviation.

The contrasts in effective density seen at various loads while at 2250 RPM may be due to the different amounts of fuel being injected, resulting in unique mixing properties. This may result in different levels of charge inhomogeneity and could ultimately dictate the manner in which particles are formed. Changes in effective density could be explained with different primary particle sizes. Smaller primary particles will result in aggregates which contain more open space than an aggregate comprised of larger primaries for a given mobility-equivalent diameter. This would give a lower mass and effective density. This agrees well with the density trends seen above, because the increase in density with load may be

explained by the fact that the larger quantity of fuel at high load does not mix as well, resulting in locally rich regions in which primary particles are able to grow larger. The addition of ethanol appears to limit this effect, and could be attributed to the oxygen on the ethanol molecule providing poorer conditions for soot nucleation.

The effective density trends produced at idle are noticeably different from the other three engine loads, having lower mass-mobility exponents and higher prefactors. This, along with the fact that many engine parameters are different while at speed versus idle (valve timing, ignition timing, etc.) suggest that idling results in dissimilar combustion in comparison to operation at higher speeds.

3.4 Mass Concentration

The SMPS scans were then combined with the number and mass volatile fractions and mass-mobility relationships to calculate the mass distributions of volatile and non-volatile material. The methodology for determining these distributions is summarized here and is given in detail by Dickau et al (2016), which is an extension of the work by Sakurai et al. (2003). For a given engine condition and fuel, the mass concentration of non-volatile PM was determined by multiplying the number size distribution by the undenuded particle mass (m_U) and introducing the number and mass volatile fractions as follows:

$$\left(\frac{\mathrm{d}M}{\mathrm{dlog}d_\mathrm{m}}\right)_{\mathrm{non-volatile}} = C_\mathrm{U} {d_\mathrm{m,U}}^{D_\mathrm{m,U}} \left(\frac{\mathrm{d}N_\mathrm{U}}{\mathrm{dlog}d_\mathrm{m,U}}\right)(1-f_\mathrm{N})(1-f_\mathrm{m}) \,, \tag{8}$$

where the mass of undenuded particles as a function of mobility size is determined by a power-law fit of the undenuded mass and mobility diameter data ($m_\mathrm{U} = C_\mathrm{U} {d_\mathrm{m,U}}^{D_\mathrm{m,U}}$). Plots of the undenuded mass and mobility diameter data and fits are shown in the supplemental information. Here f_N and f_m are the averages of the size-segregated f_N and f_m, respectively, as no dependence on size was observed. Similarly, the internally mixed volatile portion is:

$$\left(\frac{\mathrm{d}M}{\mathrm{dlog}d_\mathrm{m}}\right)_{\mathrm{internal\ volatile}} = C_\mathrm{U} {d_\mathrm{m,U}}^{D_\mathrm{m,U}} \left(\frac{\mathrm{d}N_\mathrm{U}}{\mathrm{dlog}d_\mathrm{m,U}}\right)(1-f_\mathrm{N}) f_\mathrm{m} \,. \tag{9}$$

The volatile mass concentration of externally mixed particles is

$$\left(\frac{\mathrm{d}M}{\mathrm{dlog}d_\mathrm{m}}\right)_{\mathrm{external\ volatile}} = \rho_0 \left(\frac{\pi}{6} {d_\mathrm{m,U}}^3\right)\left(\frac{\mathrm{d}N_\mathrm{U}}{\mathrm{dlog}d_\mathrm{m,U}}\right) f_\mathrm{N} \,, \tag{10}$$

where ρ_0 is the density of the externally mixed volatile material assuming the particles are spherical. As density of these particles is not explicitly known, it was assumed they had a density of 1000 kg/m^3. Since the fraction of externally mixed volatile particles was relatively low, this assumption has little effect on the total calculated mass concentration.

An example mass distribution is given in Figure 9 using E0 at 4% load. The data itself is plotted where possible (i.e. below 225 nm, the upper limit of the SMPS range). An equation comprised of two log-normal distributions was fit to the mass data and is used to extrapolate the mass distribution above 225 nm as shown in the figure. This was done in an effort to represent the mass distribution without missing a portion of the mass found at larger mobility-equivalent diameters.

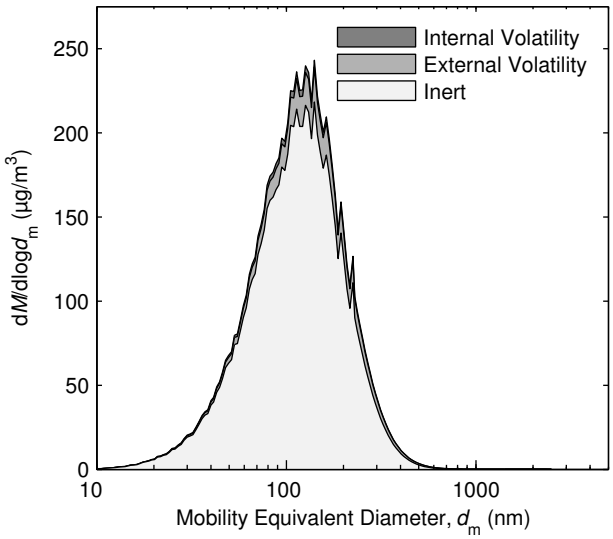

Figure 9: Mass distribution of volatile and non-volatile material at 4% load using E0. The components are graphed additively; the actual value of each component is given by the difference between its curve and the curve below it.

The internally and externally mixed volatile mass concentrations can be combined using the formula

$$M_{\text{volatile}} = \sum \begin{pmatrix} C_{\text{U}} {d_{\text{m,U}}}^{D_{\text{m,U}}} \left(\frac{\text{d}N_{\text{U}}}{\text{dlog}d_{\text{m,U}}}\right)(\text{dlog}d_{\text{m,U}})(1-f_{\text{N}})f_{\text{m}} \\ +\rho_0 \left(\frac{\pi}{6} {d_{\text{m,U}}}^3\right)\left(\frac{\text{d}N_{\text{U}}}{\text{dlog}d_{\text{m,U}}}\right)(\text{dlog}d_{\text{m,U}})f_{\text{N}} \end{pmatrix}, \quad (11)$$

where M_{volatile} is the total mass concertation of volatile material. The mass concentration of non-volatile material ($M_{\text{non-volatile}}$) is determined as

$$M_{\text{non-volatile}} = \sum C_{\text{U}} {d_{\text{m,U}}}^{D_{\text{m,U}}} \left(\frac{\text{d}N_{\text{U}}}{\text{dlog}d_{\text{m,U}}}\right)(\text{dlog}d_{\text{m,U}})(1-f_{\text{N}})(1-f_{\text{m}}) \, . \quad (12)$$

The volatile and non-volatile masses for all fuel and engine conditions are displayed in Figure 10. Because both f_{N} and f_{m} are similar between all engine conditions and fuels, the volatile mass concentration tends to scale with number concentration seen in Figure 7. Most differences between the two plots can be attributed to variations in size distributions (GMD), which have a large effect on mass concentration. For example, the number concentrations from idle and 13% load are similar, but between the two conditions, idle has the lower mass concentration due to its lower GMD.

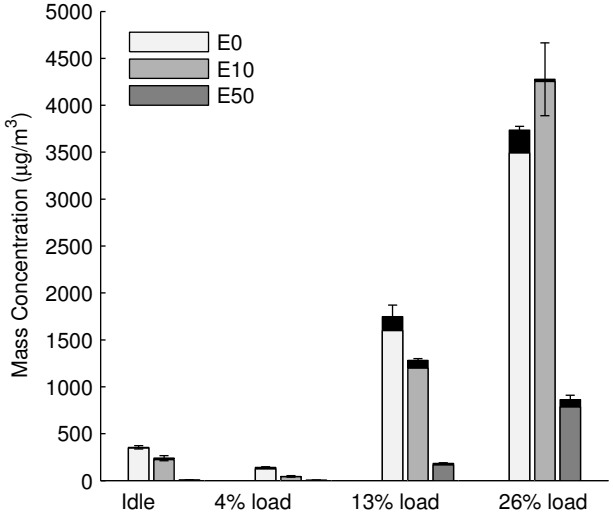

Figure 10: Mass concentration of volatile and non-volatile PM. Error bars represent one standard deviation in total mass concentration, black regions depict volatile material and other shades are non-volatile material.

4. Conclusion

The particulate matter from a GDI engine fuelled with ethanol blends has been characterized by its volatility, size distribution, mass-mobility exponent, and effective density. In general, particle number concentration increased with engine load, but idle produced approximately the same number concentrations as 13% load. In terms of mass concentration, the idle condition produced approximately the same as the 4% load. Number and mass concentrations generally decreased with ethanol fraction, although E10 produced marginally higher number concentrations than E0 at idle and 26% load. Size distributions were not log-normal and were skewed. Both the number volatile fraction and mass volatile fraction were under 10 percent in all instances. Mass-mobility exponent ranged from 2.28 to 2.60. Ethanol fraction and engine load were found to have statistically significant effects on effective density. Ethanol fraction tended to decrease effective density and mass-mobility exponent, except at idle. Effective density and mass-mobility exponent increased with load.

The results show that blending ethanol with gasoline could be an effective method of reducing GDI particulate emissions. While some statistically significant changes in PM morphology attributable to ethanol (i.e. reductions in effective density and mass-mobility exponent) have been observed, these changes are relatively small and so particle mitigation strategies used for GDI engines fuelled on pure gasoline may not need to be adapted dramatically to suit engines fuelled on ethanol blends. Very little volatility has been observed for this engine, and so a gasoline particulate filter would be a logical next step if further reduction in PM output is desired.

Acknowledgements

Daniel Stang is gratefully acknowledged for his work in setting up the engine. Funding for this project was provided by the AUTO21 and NSERC grant programs.

Supplemental Material

Supplemental data is available on the publisher's website.

References

Barone, T., Storey, J., Youngquist, A., and Szybist, J. (2012). An Analysis of Direct-Injection Spark-Ignition (DISI) Soot Morphology. *Atmospheric Environment*. 49: 268–274.

Bielaczyc, P., Woodburn, J., and Szczotka, A. (2014). Particulate Emissions from European Vehicles Featuring Direct Injection Spark Ignition Engines Tested Under Laboratory Conditions. *SAE International Journal of Fuels and Lubricants*. 7(2): 580–590.

Bonatesta, F., Chiapetta, E., and La Rocca, A. (2014). Part-Load Particulate Matter from a GDI Engine and the Connection with Combustion Characteristics. *Applied Energy*. 124: 366–376.

California Air Resources Board (CARB). (2015). An Update on the Measurement of PM Emissions at LEV III Levels. Technical Support Document. Sacramento, CA.

Catapano, F., Di Iorio, S., Lazzaro, M., Sementa, P., and Vaglieco, B. (2013). Characterization of Ethanol Blends Combustion Processes and Soot Formation in a GDI Optical Engine. *SAE International*. Doi: 10.4271/2013-01-1316.

Chen, L., Braisher, M., Crossley, A., Stone, R., and Richardson, D. (2010). The Influence of Ethanol Blends on Particulate Matter Emissions from Gasoline Direct Injection Engines. *SAE International*. Doi: 10.4271/2010-01-0793.

Chen, L., Stone, R., and Richardson, D. (2012). Effect of the Valve Timing and the Coolant Temperature on Particulate Emissions from a Gasoline Direct-Injection Engine Fuelled with Gasoline and with a Gasoline–Ethanol Blend. *Proceedings of the Institution of Mechanical Engineers, Part D: Journal of Automobile Engineering*. Doi: 10.1177/0954407012444966.

Chen, L., Zhang, Z., Gong, W., and Liang, Z. (2015). Quantifying the Effects of Fuel Compositions on GDI-Derived Particle Emissions using the Optimal Mixture Design of Experiments. *Fuel*. 154: 252–260.

Dastanpour, R., and Rogak, S. N. (2014). Observations of a Correlation between Primary Particle and Aggregate Size for Soot Particles. *Aerosol Science and Technology*. 48(10): 1043–1049.

Dastanpour, R., Rogak, S., Graves, B., Olfert, J. S., Eggersdorfer, M., and Boies, A. (2015). Improved Sizing of Soot Primary Particles using Mass-Mobility Measurements. *Aerosol Science and Technology*. 50(2): 101–109.

Dickau, M., Olfert, J. S., Stettler, M., Boies, A., Momenimovahed, A., Thompson, K., Smallwood, G., Johnson, M. (2016). Methodology for Quantifying the Mixing State of an Aerosol. *Aerosol Science and Technology*. 50(8): 759–772.

Energy Information Administration (EIA). Biofuels Issues and Trends. U.S. Department of Energy. Washington DC. October, 2012.

Energy Information Administration (EIA). How Much Ethanol is Produced, Imported, and Consumed in the United States?. http://www.eia.gov/tools/faqs/faq.cfm?id=90&t=4. Updated April 7, 2015. Accessed July 20, 2015.

Energy Information Administration (EIA). Short-Term Energy Outlook (STEO) July 2015. U.S. Department of Energy. Washington DC. July, 2015.

Farron, C., Matthias, N., Foster, D., Andrie, M., Krieger, R., Najt, P., Narayanaswamy, K., Solomon, A., and Zelenyuk, A. (2011). Particulate Characteristics for Varying Engine Operation in a Gasoline Spark Ignited, Direct Injection Engine. *SAE International*. Doi: 10.4271/2011-01-1220.

Fatouraie, M., Wooldridge, M., and Wooldridge, S. (2013). In-Cylinder Particulate Matter and Spray Imaging of Ethanol/ Gasoline Blends in a Direct Injection Spark Ignition Engine. *SAE International Journal of Fuels and Lubricants*. Doi: 10.4271/2013-01-0259.

Ghazi, R., Tjong, H., Soewono, A., Rogak, S. N., and Olfert, J. S. (2013). Mass, Mobililty, Volatility, and Morphology of Soot Particles Generated by a McKenna and Inverted Burner. *Aerosol Science and Technology*. 47(4):395–405.

Giechaskiel, B., Carriero, M., Martini, G., Krasenbrink, A., and Scheder, D. (2009). Calibration and Validation of Various Commercial Particle Number Measurement Systems. *SAE International Journal of Fuels and Lubricants.* 2(1): 512–530.

Graves, B., Olfert, J., Patychuk, B., Dastanpour, R., and Rogak, S. (2015). Characterization of Particulate Matter Morphology and Volatility from a Compression-Ignition Natural Gas Direct-Injection Engine. *Aerosol Science and Technology*. 49(8): 589–598.

Gu, X., Huang, Z., Cai, J., Gong, J., Wu, X., and Lee, C. (2012). Emission Characteristics of a Spark-Ignition Engine Fuelled with Gasoline-n-Butanol Blends in Combination with EGR. *Fuel*. 93: 611–617.

Kameya, Y., and Lee, K. (2013). Ultra-Small-Angle X-ray Scattering Characterization of Diesel/Gasoline Soot: Sizes and Particle-Packing Conditions. *Journal of Nanoparticle Research*. Doi: 10.1007/s11051-013-2006-6.

Karavalakis, G., Short, D., Vu, D., Villila, M., Asa-Awuku, A., and Durbin, T. (2014a). Evaluating the Regulated Emissions, Air Toxics, Ultrafine Particles, and Black Carbon from SI-PFI and SI-DI Vehicles Operating on Different Ethanol and Iso-Butanol Blends. *Fuel.* 128: 410–421.

Khalek, I., Bougher, T., and Jetter, J. (2010). Particle Emissions from a 2009 Gasoline Direct Injection Engine Using Different Commercially Available Fuels. *SAE International Journal of Fuels and Lubricants*. 3(2): 623–637.

Kim, Y. [Yongha], Kim, Y. [Youngjae], Kang, J., Jun, S., Rew, S., and Lee, D. (2013). Fuel Effect on Particle Emissions of a Direct Injection Engine. *SAE International*. Doi: 10.4271/2013-01-1559.

Lee, K., Seong, H., Sakai, S., Hageman, M., and Rothamer, D. (2013). Detailed Morphological Properties of Nanoparticles from Gasoline Direct Injection Engine Combustion of Ethanol Blends. *SAE International*. Doi: 10.4271/2013-24-0185.

Liang, B., Ge, Y., Tan, J., Han, X., Gao, L., Hao, L., Ye, W., and Dai, P. (2013). Comparison of PM Emissions from a Gasoline Direct Injected (GDI) Vehicle and a Port Fuel Injected (PFI) Vehicle Measured by Electrical Low Pressure Impactor (ELPI) with Two Fuels: Gasoline and M15 Methanol Gasoline. *Journal of Aerosol Science*. 57: 22–31.

Liu, Z., Swanson, J., Kittleson, D., and Pui, D. (2012). Comparison of Methods for Online Measurement of Diesel Particulate Matter. *Environmental Science and Technology*. 46(11): 6127–6133.

Maricq, M., Podsiadlik, D., Brehob, D., and Haghgooie, M. (1999). Particulate Emissions from a Direct-Injection Spark-Ignition (DISI) Engine. *Proceedings of the SAE International Spring Fuels and Lubricants Meeting*. Dearborn, MI.

Maricq, M., and Xu, N. (2004). The Effective Density and Fractal Dimension of Soot Particles from Premixed Flames and Motor Vehicle Exhaust. *Journal of Aerosol Science*. 35: 1251–1274.

Maricq, M., Szente, J., and Jahr, K. (2012). The Impact of Ethanol Fuel Blends on PM Emissions from a Light-Duty GDI Vehicle. *Aerosol Science and Technology*. 46(5): 576–583.

Momenimovahed, A., and Olfert, J. S. (2015). Effective Density and Volatility of Particles Emitted from Gasoline Direct Injection Vehicles and Implications for Particle Mass Measurement. *Aerosol Science and Technology*. *49: 1051–1062.*

Olfert, J. S., and Collings, N. (2005). New Method for Particle Classification—The Couette Centrifugal Particle Mass Analyzer. *Journal of Aerosol Science.* 36(11): 1338–1352.

Olfert, J. S., Symonds, J., and Collings, N. (2007). The Effective Density and Fractal Dimension of Particles Emitted from a Light-Duty Diesel Vehicle with a Diesel Oxidation Catalyst. *Journal of Aerosol Science*. 38: 69–82.

Park, K., Cao, F., Kittelson, D., and McMurry, P. (2003). Relationship between Particle Mass and Mobility for Diesel Exhaust Particles. *Environmental Science and Technology*. 37(3): 577–583.

Quiros, D., Hu, S. [Shaohua], Hu, S. [Shishan], Lee, E., Sardar, S., Wang, X., Olfert, J. Jung, H., Zhu, Y., and Huai, T. (2015). Particle Effective Density and Mass During Steady-State Operation of GDI, PFI, and Diesel Passenger Cars. *Journal of Aerosol Science*. 83: 39–54.

Ristimäki, J., Vaaraslahti, K., Lappi, M., and Keskinen, J. (2007). Hydrocarbon Condensation in Heavy-Duty Diesel Exhaust. Environmental Science and Technology. 41:6397–6402.

Samuel, S., Hassaneen, A., and Morrey, D. (2010). Particulate Matter Emissions and the Role of Catalytic Converter During Cold Start of GDI Engine. *SAE International*. Doi: 10.4271/2010-01-2122.

Sakurai, H., Park, K., McMurry, P., Zarling, D., Kittleson, D., and Ziemann, P. (2003) Size-Dependent Mixing Characteristics of Volatile and Nonvolatile Components in Diesel Exhaust Aerosols. *Environmental Science and Technology*. 37(24): 5487–5495.

Seong, H., Choi, S., and Lee, K. (2014). Examination of Nanoparticles from Gasoline Direct-Injection (GDI) Engines using Transmission Electron Microscopy (TEM). International *Journal of Automotive Technology*. 15(2): 175–181.

Sgro, L. A., Sementa, P., Vaglieco, B. M., Rusciano, G., Andrea D'Anna, A., and Minutolo, P. (2012). Investigating the Origin of Nuclei Particles in GDI Engine Exhausts. *Combustion and Flame*. 159: 1687–1692.

Short, D., Vu, D., Durbin, T., Karavalakis, G., and Asa-Awuku, A. (2015). Particle speciation of Emissions from iso-butanol and ethanol blended gasoline in light-duty Vehicles. *Journal of Aerosol Science*. 84: 39–52.

Stolzenburg, M., and McMurry, P. (2008). Equations Governing Single and Tandem DMA Configurations and a New Lognormal Approximation to the Transfer Function. *Aerosol Science and Technology*. 42(6): 421–432.

Stone, R. (2012). Introduction to Internal Combustion Engines, 4th Edition. Palgrave Macmillan. Basingstoke, UK.

Storey, J., Barone, T., Norman, K., and Lewis, S. (2010). Ethanol Blend Effects On Direct Injection Spark-Ignition Gasoline Vehicle Particulate Matter Emissions. *SAE International Journal of Fuels and Lubricants*. Doi: 10.4271/2010-01-2129.

Storey, J., Barone, T., Thomas, J., and Huff, S. (2012). Exhaust Particle Characterization for Lean and Stoichiometric DI Vehicles Operating on Ethanol-Gasoline Blends. *SAE International*. Doi: 10.4271/2012-01-0437.

Storey, J., Lewis, S., Szybist, J., Thomas, J., Barone, T., Eibl, M., Nafziger, E., and Kaul, B. (2014). Novel Characterization of GDI Engine Exhaust for Gasoline and Mid-Level Gasoline-Alcohol Blends. *SAE International Journal of Fuels and Lubricants*. Doi: 10.4271/2014-01-1606.

Su, J., Lin, W., Sterniak, J., Xu, M., and Bohac, S. (2013). Particulate Matter Emission Comparison of Spark Ignition Direct Injection (SIDI) and Port Fuel Injection (PFI) Operation of a Boosted Gasoline Engine. *Proceedings of the ASME 2013 Internal Combustion Engine Division Fall Technical Conference*. Dearborn, MI.

Symonds, J., Price, P., Williams, P., and Stone, R. (2008). Density of Particles Emitted from a Gasoline Direct Injection Engine. *Proceedings of the European Aerosol Conference*. Thessaloniki, Greece.

Tajima, N., Fukushima, N., Ehara, K. and Sakurai, H. (2011). Mass Range and Optimized Operation of the Aerosol Particle Mass Analyzer. *Aerosol Science and Technology*. 45(2): 196–214.

United Nations Economic Comission for Europe (UNECE). E/ECE/324/Rev.2/Add.100/Rev.3. Agreement Concerning the Adoption of Uniform Technical Prescriptions for Wheeled Vehicles, Equipment

and Parts Which can be Fitted and/or be Used on Wheeled Vehicles and the Conditions for Reciprocal Recognition of Approvals Granted on the Basis of these Prescriptions. August, 2013.

U.S. Department of Energy. Ethanol Vehicle Emissions. http://www.afdc.energy.gov/vehicles/flexible_fuel_emissions.html. Accessed August 25, 2015.

Vuk, C., and Vander Griend, S. (2013). Fuel Property Effects on Particulates In Spark Ignition Engines. *SAE International*. Doi: 10.4271/2013-01-1124.

Whelan, I., Timoney, D., and Smith, W. (2013). The Effect of a Three-Way Catalytic Converter on Particulate Matter from a Gasoline Direct-Injection Engine During Cold- Start. *SAE International Journal of Fuels and Lubricants*. Doi: 10.4271/2013-01-1305.

Zhang, Z., Wang, T., Jia, M., Wei, Q., Meng, X., and Shu, G. (2014). Combustion and Particle Number Emissions of a Direct Injection Spark Ignition Engine Operating on Ethanol/Gasoline and n-Butanol/Gasoline Blends with Exhaust Gas Recirculation. *Fuel*. 130: 177–188.